Korean J. Chem. Eng., 35(10), 2078-2085 (2018)
DOI: 10.1007/s11814-018-0105-x

pISSN: 0256-1115
eISSN: 1975-7220

Removal of Zn (II) by complexation-ultrafiltration using rotating disk membrane and the shear stability of PAA-Zn complex

Shuyun Tang and Yunren Qiu†

School of Chemistry and Chemical Engineering, Central South University, Changsha 410083, China
(*Received 8 April 2018 • accepted 13 June 2018*)

Abstract−Polyacrylic acid sodium (PAAS) was applied to remove Zn (II) from aqueous solutions by complexation-ultrafiltration using a rotating disk membrane module. As important factors, solution pH and the mass ratio of polymer to metal ions (P/M) on the rejection of Zn (II) were investigated, and the rejection could reach to 95.3% at pH=7, P/M=25 and 500 rpm. In addition, a partition model was proposed to reveal instability mechanism of the PAA-Zn complex in the shear field for the first time. The critical rotating speeds at which PAA-Zn complexes begin to dissociate were 1,460, 1,390, 1,280 rpm at pH 7.0, 6.0, 5.0, respectively. The corresponding critical shear rates (γ_c), the smallest shear rates at which PAA-Zn complex begins to dissociate, were 1.58×10^5, 1.45×10^5 and 1.25×10^5 s^{-1} at pH 7.0, 6.0, 5.0, respectively. In addition, the relationship between the critical radii and the critical rotating speed was obtained.

Keywords: Critical Shear Rate, Complexation-ultrafiltration, Rotating Disk Membrane, Dynamic Ultrafiltration, Shear Stability

INTRODUCTION

Large volume of wastewater containing Zn (II) is created in the production of zinc manufacturing and other industries such as electroplating and insecticides [1]. Trace amounts of Zn (II) are necessary for life [2], but a great extra amount of Zn (II) is toxic, which can cause irritability, muscular stiffness, lung disorders, loss of appetite, nausea and even cancer [3,4]. The World Health Organization (WHO) recommends a level of zinc in drinking water below 3 mg L^{-1} [5]. The treatment of heavy metals, especially for low-level heavy metals, has attracted great interest in the past few years [6-8]. Conventional treatment methods of heavy metals generally include chemical precipitation, adsorption, ion-exchange and reverse osmosis, etc., which have obvious disadvantages, such as the high-energy requirements especially when the heavy metal concentration is less than 100 mg L^{-1}, the production of sludge, which is secondary contamination, falls short of quality of the treated water within acceptable limits [9-11].

Membrane separation has been proposed as an alternative to greatly improve the removal efficiency and decrease operation consumption [12,13]. Complexation-ultrafiltration, also called polymer enhanced ultrafiltration (PEUF), which uses water-soluble polymers as complex agents, has been considered as an excellent method of heavy metal treatment, especially for those with low concentration of heavy metals [14-18]. Previous study showed that poly (acrylic acid) sodium (PAAS) has been widely used in PEUF due to its good water solubility and high affinity towards heavy metal ions [15,19,20].

Although PEUF presents great potential for the treatment of wastewater containing heavy metals and the removal efficiency of heavy metal is more than 95% in laboratory [14,15], and more researchers focus on the removal efficiency influenced by the pH, mass ratio of polymer to metal and background electrolytes with various complexing agents [14,20,21], the industrial application of PEUF is rarely reported. As previous report, a pilot plant was designed by the Canadian Atomic Energy Research Institute [22] to treat heavy metal elements in wastewater, but the removal efficiency was only ~40%, which is far less than that in the laboratory. A similar result was obtained by our pilot experiment;, the removal efficiency of Zn (II) dropped from ~95% (using peristaltic pump) to only ~45% (using centrifugal pump). The only difference is that a different pump was used. The rapid decrease of rejection may have been the dissociation of the PAA-Zn complex. The high shear rate, caused by the blades of the centrifugal pump, would destroy the bond of carboxyl-Zn and lead the PAA-Zn complex to dissociate, which results in a remarkable decline of the removal efficiency. This means that the PAA-Zn complex may dissociate when the shear rate exceeds a certain value.

To take advantage of PEUF and promote its industrial application, the stability of PAA-Zn complex must be investigated in the shear field. The shear rate was generated by a rotating disk on the ultrafiltration membrane surface to study the shear stability of polymer-metal complexes in our laboratory. Until now, the rotating disk membrane filtration has been successfully applied for the purification and separation of various products, such as microalgae [23,24], fine particles in seawater [25], leaf protein [26], sugar beet juice [27] and milk proteins [28,29]. However, the removal of Zn (II) by complexation-ultrafiltration using rotating disk membrane module and the shear stability of PAA-Zn complex are relatively unexplored.

We used the rotating disk with six rectangular vanes to simulate a centrifugal pump impeller to study the shear stability of PAA-Zn complex at different pHs for the first time. A partition model was

†To whom correspondence should be addressed.
E-mail: csu_tian@csu.edu.cn

proposed to predict the radial distribution of substances on the membrane surface. The stability of PAA-Zn complex in the shear field was investigated for the first time. The critical rotating speed at which PAA-Zn complex begins to dissociate and the corresponding critical shear rate, the smallest shear rate at which PAA-Zn complex begins to dissociate, was calculated, which could give guidance for the selection of delivery pump and rotating speed to avoid the polymer-metal complex from dissociating, and ensure effective removal of the Zn (II) in the industrial application of PEUF. The stability of the PAA-Zn complex is not influenced by the centrifugal pump at low speed or diaphragm pump or other low-shear pumps, which greatly improves the efficiency of complexation-ultrafiltration in industry.

MATERIALS AND METHOD

1. Materials

All reagents were reagent grade products. Macro-molecular metal complexes were prepared by poly (acrylic acid) sodium (PAAS) and zinc chloride ($ZnCl_2$) in ultrapure water (prepared by ultrafiltration and reverse osmosis). The poly (acrylic acid) sodium (PAAS) with average molecular weight 250 kDa (Wako Pure Chemical Industries, Ltd., Japan) was used as a complexing agent. The Zn (II) concentrations in permeate and retentate were measured by atomic absorption spectrophotometry at 213.8 nm. Fluid viscosity was measured using Ubbelohde viscometer. $ZnCl_2$ solution with the concentration of 0.01 g L^{-1} was used as simulation wastewater. The pH of the feed solution was adjusted by adding hydrochloric acid (0.1 M) or sodium hydroxide (0.1 M). Ultrapure water was used throughout the experimental runs.

2. Membranes, Experimental Set-up and Ultrafiltration Experiments

The filtration test set-up is represented in Fig. 1(a). The feed stream is circulated from a 4 L thermostatic to the filtration chamber tank by a peristaltic pump at a flow-rate 30 L/h. Feed inlet is located at 3 cm from center on the bottom while the retentate outlet is placed at the center on the top of the housing. The permeate is collected from a port at 2 cm from center on the top plate into a beaker which is placed on an electronic scale to calculate the variations of the permeate mass. To explore the relationship between the theoretical pressure and the experimental pressure, and then further investigate the pressure distribution on the membrane surface, the pressure measurements were evenly carried out at three points in the membrane radius direction: r=0.029, 0.059 m and the housing periphery (0.088 m), respectively. The PES (polyethersulfone) flat ultrafiltration membranes, a modified hydrophilic membrane, were purchased from Shanghai Yuling Filtration Equipment Co., Ltd. The parameters of the flat membrane are given in Table 1. The rotating disk membrane set-up is shown in Fig. 1(b). The filtration module consists of an 88 mm inner radius circular housing inside with a disk rotating which can speed up to 3,000 rpm adjustable around a shaft. The rotating disk membrane (RDM) is made up of a rotating disk and the fixed membrane. The disk with six rectangular vanes is rotatable, the membrane is put on the front circular plate of the housing opposite the shaft, and it is immobile. The rotating disk can produce shear rate on the membrane surface to lessen the fouling of the membrane surface and enhance the filtration. The axial gap between membrane and disk is 14 mm, while the disk radius and thickness are 83 mm and 4 mm, respectively.

Table 1. The parameters of the flat membrane

Membrane type	Molecular weight cut-off (kDa)	r_m (mm)	r_0 (mm)	Surface area (m^2)
Polyethersulfone (PES)	30	180	14	0.0253

3. Titrations of the PAAS

The 100 mg/L PAAS solution was prepared by dissolving the PAAS in the deionized water. A volume of 2 ml HCl (0.1 M) was added at the beginning of the experiment to lower the pH to approximately 4.0. Titrations were carried out by stepwise addition of 0.25 ml of 0.1096 M NaOH (standardized by potassium acid phthalate) to the flask placed in the thermostatic cell (25 °C). The pH value and conductivity were measured using a pH meter (PHS-3C, from Shanghai Precision & Scientific Instrument Co. Ltd.) and conductivity meter (DDS-11A, Lei-Ci), respectively. Titration curves provided ways to estimate the concentration of the carboxylic group [14].

4. The Calculation of Critical Shear Rate and Critical Shear Radius

The rejection of metal ions showing the separation properties in the complexation-ultrafiltration process is given by the formula:

$$R=1-C_p/C_f \quad (1)$$

where C_p and C_f are the Zn(II) concentrations of the permeate and the feed, respectively.

The shear rates on the membrane surface γ_m were calculated by

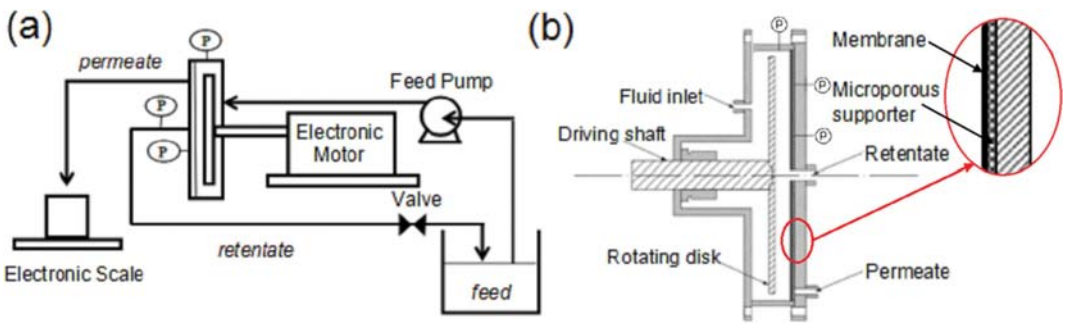

Fig. 1. Schematic of (a) experiment set-up (b) rotating disk membrane.

Bouzerar et al. [30], who solved the axisymmetric Navier-Stokes equations using the similarity solution of Bödewadt in the laminar regime (N<570 rpm) and turbulent regime (N>570 rpm). The results were found as in laminar flow

$$\gamma_{ml}=0.77\upsilon^{-0.5}(k\omega)^{1.5}r \tag{2}$$

in turbulent flow

$$\gamma_{mt}=0.0296\upsilon^{-0.8}(k\omega)^{1.8}r^{1.6} \tag{3}$$

where υ is kinematic viscosity (m^2s^{-1}). ω is the disk angular velocity (rad/s), r is the radius (m), k is induced velocity factor [31]. According to Itoh et al., k in the rotating disk is independent of the radius [32], and determined by peripheral pressure at different speeds, satisfying Bernoulli equation in the inviscid core:

$$P_p=0.0055\rho k^2N^2r^2+P_0 \tag{4}$$

where N is the rotating speed (rpm), ρ is the density (kg m^{-3}), P_0 is the center pressure (Pa), which is equal to the peripheral pressure at N=0.

The shear rate increases with the increase of radius. Polymer-metal complexes may dissociate when the energy generated by the shear rate is greater than the bonding energy of polymer-metal. The distribution map of substances on the membrane surface is shown in Fig. 2(a). The critical shear radius (r_c) is the radius where polymer-metal complexes begin to dissociate. When the $r_0 \le r < r_c$, the polymer-metal complexes are stable and can be retained by membrane, and the concentration of the metal ions in the permeate is equal to the concentration of the free metal ions (C_0). When $r_c \le r < r_m$, polymer-metal complexes are completely dissociated, and the concentration of the metal ions in the permeate is equal to the initial metal ions concentration (C_f). The shear rate generated by the rotating disk at the critical radius of membrane is called as critical shear rate (γ_c) of the polymer-metal complex; it is also the smallest shear rate for the polymer-metal complex to dissociate. Here r_m is the membrane outside radius and r_0 is the membrane inside radius.

According to mass balance equation,

$$V_p=V_{com}+V_{dis} \tag{5}$$

$$V_pC_p=V_{com}C_{com}+V_{dis}C_{dis} \tag{6}$$

the metal ion concentration C_p and the volume V_p of permeate can be obtained by the experiments. C_{dis}, C_{com} and V_{dis}, V_{com} represent the metal ion concentrations and volume of permeate in the dissociation and complexation regions, respectively.

A partition model of the membrane Fig. 2(b) is proposed to predict the volumes of the permeate (V_{dis} and V_{com}). In this model, an annular ring membrane between the inner radius r_i and the outer radius r_{i+1} was prepared for studying the radial distribution of permeate concentration and flux. V_i is the permeate volume of the i^{th} ring can be calculated by the permeate flux J_i [$m^3/(m^2\ s)$].

$$V_i=J_it2\pi r_i(r_{i+1}-r_i)=J_it2\pi r_i\Delta r_i \tag{7}$$

where t is the filtration time; the permeate in the both dissociation and complexation regions can be expressed by the following equations when the length of the segments (Δr_i) approaches 0:

$$V_{com}=\lim_{\Delta r_i\to 0}\sum_{i=1}^{c}2\pi tJ_ir_i\Delta r_i=2\pi t\int_{r_0}^{r_c}Jrdr \tag{8}$$

$$V_{dis}=\lim_{\Delta r_i\to 0}\sum_{i=c}^{n}2\pi tJ_ir_i\Delta r_i=2\pi t\int_{r_c}^{r_m}Jrdr \tag{9}$$

According to Darcy's law, the membrane permeate flux is linearly related to the membrane pressure, and the relationship can be expressed as

$$J_i=P_i/(\mu R_p) \tag{10}$$

$$R_t=R_m+R_f+R_c \tag{11}$$

where P_i is pressure on the membrane surface of the i^{th} ring (Pa), μ is the dynamic viscosity of the solution (Pa·s), R_t is the total resistance (m^{-1}), R_m is the membrane resistance (m^{-1}) (determined by pure water experiment), R_f is the membrane fouling (m^{-1}) and R_c is the concentration polarization resistance (m^{-1}).

V_{dis} and V_{com} can be calculated as follows:

$$V_{com}=\frac{2\pi t}{\mu R_p}\int_{r_0}^{r_c}(P_0+0.0055\rho k^2N^2r^2)rdr \tag{12}$$

$$V_{dis}=\frac{2\pi t}{\mu R_p}\int_{r_c}^{r_m}(P_0+0.0055\rho k^2N^2r^2)rdr \tag{13}$$

Combining with Eq. (6):

$$\begin{aligned}V_pC_p=&\frac{2\pi tC_0}{\mu R_p}\int_{r_0}^{r_c}(P_0+0.0055\rho k^2N^2r^2)rdr\\&+\frac{2\pi tC_f}{\mu R_p}\int_{r_c}^{r_m}(P_0+0.0055\rho k^2N^2r^2)rdr\end{aligned} \tag{14}$$

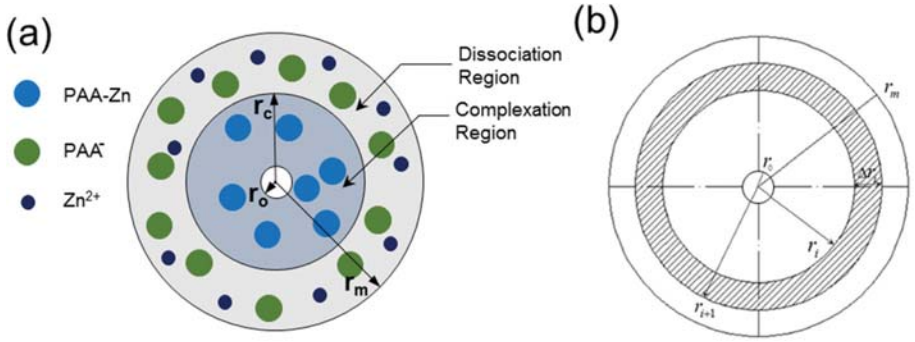

Fig. 2. (a) The distribution map of substances on the membrane surface; (b) characteristics of zone segmentation on membrane surface.

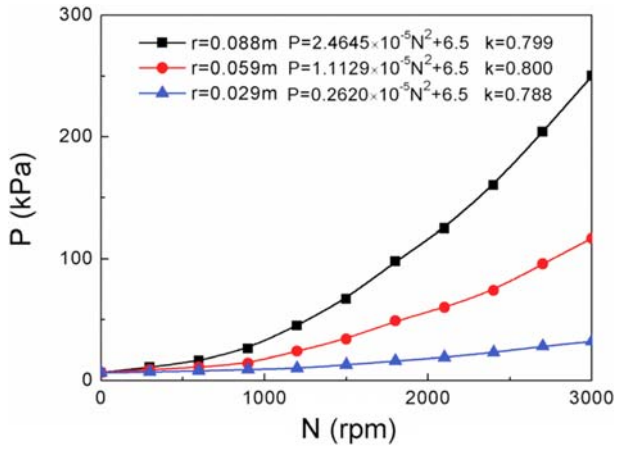

Fig. 3. Variations of pressures on the membrane surface with rotating speed (pH, 7.0; initial Zn (II) concentrations, 10 mg L^{-1}; initial PAAS concentration, 250 mg L^{-1}; temperature, 25 °C; initial pressure, 10 kPa).

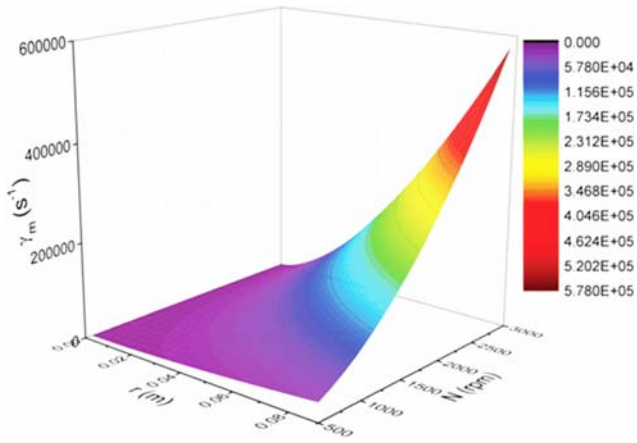

Fig. 4. The shear rate distribution map on the membrane surface.

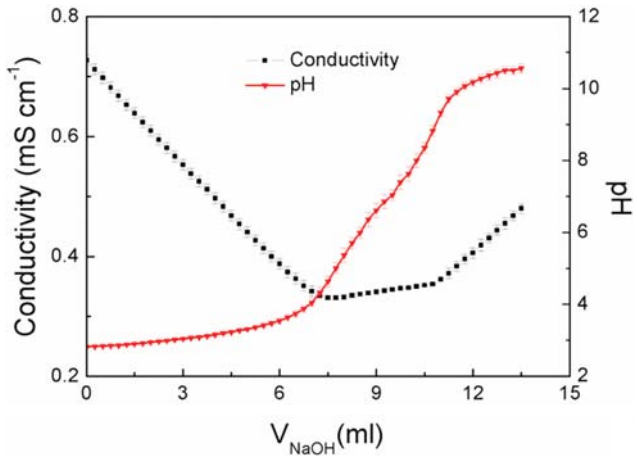

Fig. 5. Potentiometric and conductimetric titrations of PAA (initial PAAS concentration, 250 mg L^{-1}; temperature, 25 °C).

r_c can be written as:

$$r_c^4+\frac{364P_0}{\rho k^2N^2}r_c^2+\frac{C_p-C_f}{C_f-C_0}\left(r_m^4+\frac{364P_0}{\rho k^2N^2}r_m^2\right)+\frac{C_0-C_p}{C_f-C_0}\left(r_0^4+\frac{364P_0}{\rho k^2N^2}r_0^2\right)=0 \quad (15)$$

The critical radius r_c can be obtained according to Eq. (15). Bringing the r_c into Eq. (3), the critical shear rate γ_c can be calculated. The shear rate in PEUF process must be lower than the critical shear rate to ensure the removal of metal ions completely.

RESULTS AND DISCUSSION

1. Determination of Factor k and Membrane Shear Rate

The variations of pressures with rotating speed at the radii of 0.088, 0.059 and 0.029 m are represented in Fig. 3. The center pressure is 0.01 MPa. The membrane pressure increases with the rotating speed as a quadratic function, which is consistent with Torras et al. [33]. In addition, according to Eq. (4) the pressure distribution on the membrane surface is not uniform, but increases with the radius. The peripheral pressure (r=0.088 m) increased from 0.01 MPa to 0.25 MPa as the rotating speed increased from 0 rpm to 3,000 rpm. The value of k, obtained by regression [32], varied from 0.788 to 0.800 with a mean of 0.796 for the three radial positions. Since k does not vary much with radial position, we estimated the accuracy of the determination of k to be ±0.01 and determined the k=0.796 with six rectangular vanes in our module. At a rotating speed of more than 570 rpm, the flow becomes turbulent. Eq. (3) can be simplified as

$$\gamma_m=15.53r^{1.6}N^{1.8} \quad (16)$$

According to Eq. (16), the shear rate distribution map on the membrane surface is illustrated in Fig. 4. The shear rates are positively related to the radius and the rotating speed, which agrees with Bouzerar et al. [17]. The highest shear rate is 5.78×10^5 s^{-1} at 0.088 m and 3,000 rpm.

2. Potentiometric and Conductimetric Titrations of Polyacrylic Acid

Conductimetry is a function of the sum of conductivity of H^+ and OH^- in solution as these are the most conductive ions, which is closely related to the temperature and the concentration of electrolytes in solution; thus titration was carried out under isothermal conditions (25 °C) [34]. As shown in Fig. 5, the conductivity of Polyacrylic acid (PAA) solution initially clearly decreased sharply, and conversely, the corresponding pH values declined slowly, indicating the neutralization of the hydrochloric acid (in excess). A typical transitional stage of the conductivity of PAA accompanied by a sharply increase pH values implies the consumption of the protons coming from carboxylic group. Furthermore, with the neutralization of weak acids completing, a dramatic increase of the conductivity of PAA while that of pH values is stable may be ascribed to the excess of sodium hydroxide. The concentration of the carboxylic group could be estimated by the titration curves, which is 7.672 mmol/L.

3. The Stability of PAAS in the Shear Field

To further investigate the reason for the decline of rejection,

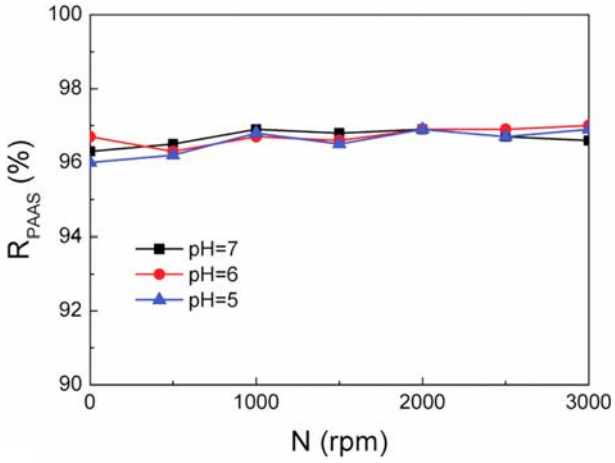

Fig. 6. Variation of the rejection of PAAS with rotating speed at various pH (initial Zn (II) concentrations, 10 mg L^{-1}; initial PAAS concentration, 250 mg L^{-1}; temperature, 25 °C; initial pressure, 10 kPa).

experiments of the stability of PAAS were performed in a shear field. The relationship between the rejection of PAAS R_{PAAS} and the rotating speed at various pH values when the concentration of PAAS is 250 mg/L is shown in Fig. 6. R_{PAAS} remains ~95% with the rotating speed changes at various pH values, only ~5% PAAS transmit to the membrane due to the existence of the low degree of polymerization of the PAAS. The results indicate that the shear rates induced from rotating disk basically have no effect on the stability of PAAS at various pH values when the rotating speed is lower than 3,000 rpm.

4. Effects of Solution pH and P/M on the Rejection of Zn (II)

To investigate the effects of solution pH and the mass ratio of polymer to metal (P/M) on rejection and permeate flux, a series of experiments were accomplished at 500 rpm. The pH is one of the most important factors in the interaction of a metal ion with a binding polymer [35]. Fig. 7 shows the effect of pH on the rejection at various P/M. Clearly, the rejection of Zn (II) is enhanced with the increasing of pH. Increasing P/M can improve the rejection of Zn (II). The rejection of Zn (II) is greater than 95.3% at the P/M=25 and pH=7.0, but the ascending tendency of rejection is not obvious with the further increase of pH. It may be that the affinity of PAAS toward Zn (II) is broken by the hydrogen positive ions at low pH, which induces the decomplexation of the PAA-Zn complex and releasing free Zn (II). The rising deprotonated carboxylic groups concentration upon the rising pH is favorable for the formation of polymer-metal complexes [16]. Therefore, the rejection of Zn (II) increases. However, it is possible that the Zn (II) is retained on the membrane at alkaline conditions due to the precipitation of $Zn(OH)_2$ [36]. The PAAS solution is alkaline due to the protonation of $[\text{-COO}]^-$ as shown in reaction (17). The complexation reaction of Zn (II) and $[\text{-COO}]^-$ is shown in reaction (18). The available bound sites for Zn (II) are fewer at a lower pH [37].

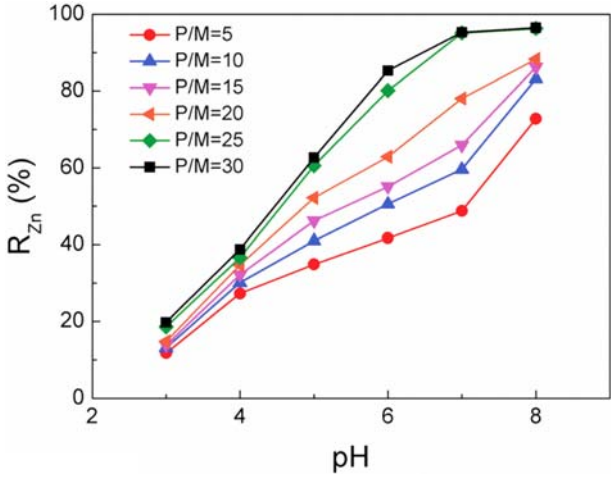

Fig. 7. Effect of pH on the rejection of Zn (II) at various P/M (initial Zn (II) concentrations, 10 mg L^{-1}; rotating speed, 500 rpm; temperature, 25 °C; initial pressure, 10 kPa).

Table 2. The viscosities, permeation coefficients and total resistances at various P/M

P/M	μ (10^{-3} Pa s)	F (m Pa^{-1} s^{-1})	μ×F (m)	R_t (m^{-1})
0	0.894	1.387×10^{-8}	1.24×10^{-11}	8.06×10^{10}
5	0.903	1.373×10^{-8}	1.24×10^{-11}	8.06×10^{10}
10	0.917	1.352×10^{-8}	1.24×10^{-11}	8.06×10^{10}
15	0.926	1.339×10^{-8}	1.24×10^{-11}	8.06×10^{10}
20	0.938	1.322×10^{-8}	1.24×10^{-11}	8.06×10^{10}
25	0.958	1.294×10^{-8}	1.24×10^{-11}	8.06×10^{10}

$$[\text{-COO}]^- + H^+ \rightleftharpoons [\text{-COOH}] \quad (17)$$

$$2[\text{-COO}]^- + Zn^{2+} \rightleftharpoons [\text{-COO}]_2Zn \quad (18)$$

The viscosities and the permeate fluxes obtained at various P/M are shown in Table 2. The permeation coefficient F (L m^{-2} kPa^{-1} h^{-1}), the permeate flux per unit pressure, has a slight decrease with the increase of P/M, which may be caused by the increase of viscosity due to the increase of the PAAS concentration, and the contributions of the membrane fouling R_f and the concentration polarization resistance R_c.

However, according to Darcy's law, it can be derived that $R_t = \Delta P/(J\mu) = 1/(F\mu)$. Table 2 reveals that R_t remains fairly constant and equals R_m (8.68×10^{10} m^{-1}), is not affected by the P/M. Thus, the slight declination of permeation coefficient F is attributed to the increase of viscosity. R_f and R_c can be neglected due to the strong shear action on the membrane surface caused by the rotating disk. During the complexation-ultrafiltration process, the permeate flux shows only ~1% decline [14,16], and the high shear rate caused by the high disk rotating speed results in a significant reduction in the membrane fouling and concentration polarization resistance [38]. Taking both rejection of Zn (II) and the permeation flux into consideration, the optimal P/M is to 25.

5. The Stability of PAA-Zn Complex in the Shear Field

The stability of the PAA-Zn complex is one of the critical factors in the complexation- ultrafiltration. Fig. 8 shows the variation of rejection of Zn (II) with rotating speed from 0 to 3,000 rpm at P/M 25 and various pHs. The rejection of Zn (II) initially remains stable due to the low rotating speed; once the speed exceeds a cer-

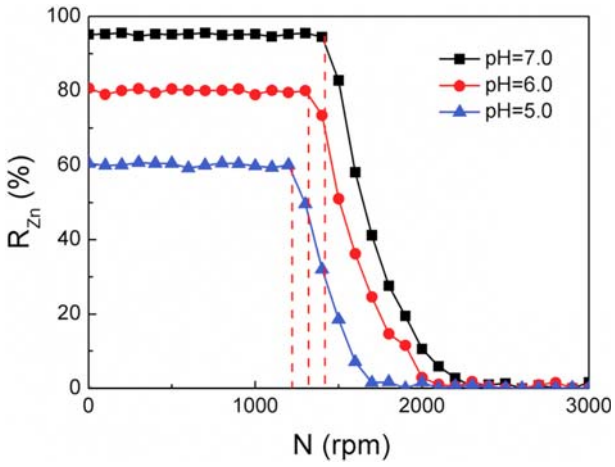

Fig. 8. Effect of rotating speed on the rejection of Zn (II) at different pH values (P/M, 25; initial Zn (II) concentrations, 10 mg L^{-1}; temperature, 25 °C; initial pressure, 10 kPa).

tain value, the rejection of Zn (II) decreases sharply. The rotating speed at which the rejection begins to decline is called the critical rotating speed, which indicates that there exists dissociation of PAA-Zn complex. The critical rotating speeds for PAA-Zn complex are 1,460, 1,390, 1,280 rpm at pH 7.0, 6.0, 5.0, respectively. As shown in Fig. 6, the molecular chain of PAAS is stable at various pH values when the rotating speed is lower than 3,000 rpm, so the rapid decrease of the Zn (II) is ascribed to the dissociation of the PAA-Zn complex, not the break of molecular chain. Fig. 9 also shows the similar characteristics, but the critical rotating speed for PAA-Zn complex to dissociate is invariable at various P/M and pH 7.0, which is ~1,460 rpm, implying the stability of the PAA-Zn bond is not affected by the P/M. Obviously, the stability of the PAA-Zn bond depends on the solution pH and the rotating speeds. At a certain pH, when the rotating speed is greater than the critical rotating speed, the PAA-Zn bond is broken and more free Zn(II) ions are released, leading to a decline of the rejection.

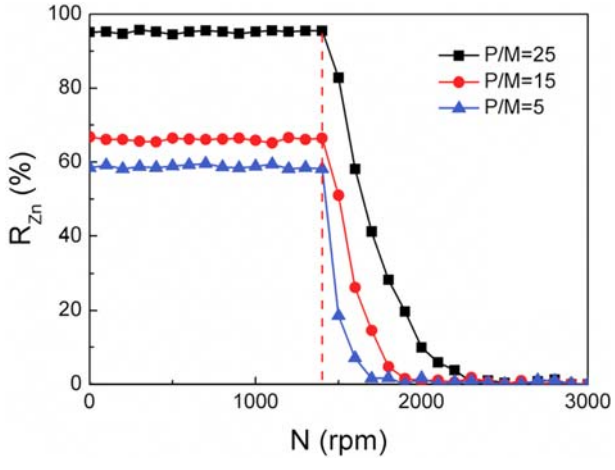

Fig. 9. Effect of rotating speed on the rejection of Zn (II) at different P/M values (pH, 7.0; initial Zn (II) concentrations, 10 mg L^{-1}; temperature, 25 °C; initial pressure, 10 kPa).

Table 3. γ_c of PAA-Zn complex and correlations of r_c and N at various pHs

pH	Nc (rpm)	γ_c (s^{-1})	Fitted curve of r_c and N
5.0	1280	1.247×10^5	$r_c=275.5N^{-1.125}$
6.0	1390	1.446×10^5	$r_c=302.3N^{-1.125}$
7.0	1460	1.580×10^5	$r_c=319.4N^{-1.125}$

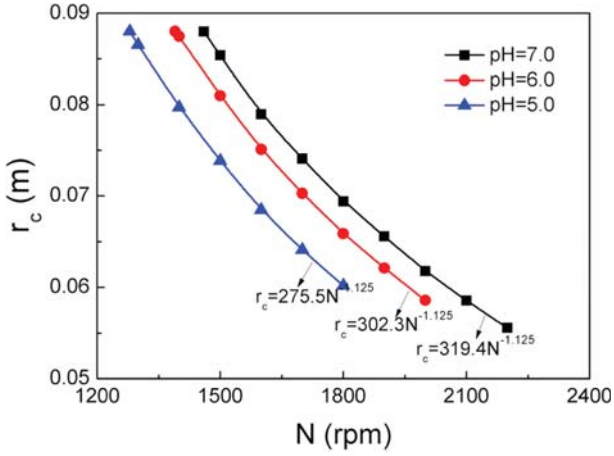

Fig. 10. The relationships between the critical radius and the rotating speed at different pH.

The critical radius is defined as the boundary within which the PAA-Zn complex can keep stable, whereas the complex at the other region will dissociate (see Fig. 2(a)). Bringing the experiment data obtained in Fig. 8 into Eq. (15), the relationship between the critical radius r_c on the membrane surface and the rotating speed N can be obtained. The correlations of r_c and N at different pH were shown in Table 3. The PAA-Zn complexes are stable and the critical shear radius cannot be obtained at low rotating speed. As shown in Fig. 10, the critical radii decreased with the increase of rotating speed at a certain pH, meaning the expansion of the scope of dissociation region. According to Table 3, the critical shear rate (γ_c) of PAA-Zn complex remains a constant at certain pH. According to Eq. (16), the shear rates are positively related to the radius and the rotating speed. The dissociation region extends from the peripheral areas to the center with the rotating speed increasing due to the constant critical shear rate of PAA-Zn complexes at a certain pH. The critical shear rates (γ_c) of PAA-Zn complexes are about 1.58×10^5, 1.45×10^5 and 1.25×10^5 s^{-1} at the pH 7.0, 6.0 and 5.0, respectively. It is obvious that the critical shear rates increase with the increase of pH. The lower pH facilitates the decomplexation of the PAA-Zn complexes, and conversely, the complexation reaction of Zn (II) and carboxylic group is enhanced. The results give guidance for delivery pump options to ensure a high removal efficiency of the Zn (II) in the industrial application of PEUF treatment for wastewater containing Zn (II).

However, the dissociated polymer and metal may complex again if they are in the lower shear field for a certain time. To make clear whether the dissociated polymer and metal may complex again or not during the membrane filtration, it is necessary to study the kinetics of the complexation of PAAS and Zn (II). Fig. 11 shows a

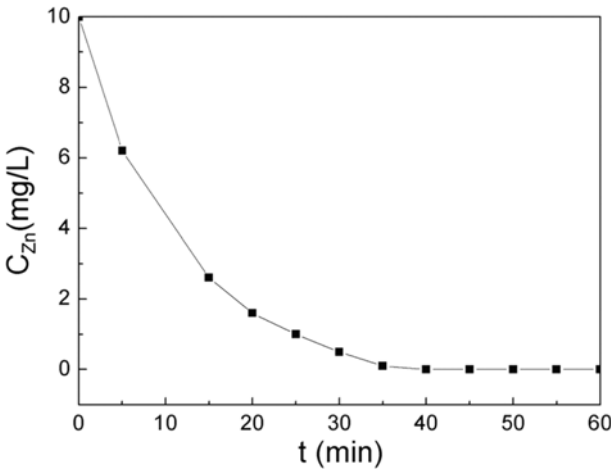

Fig. 11. Kinetic curve for the formation of PAA-Zn complex (pH 7; initial Zn (II) concentration, 10 mg L^{-1}; initial PAAS concentration, 1,000 mg L^{-1}; temperature, 25 °C; initial pressure, 10 kPa).

kinetic curve of the complex formation of PAAS with Zn (II). The kinetics experiment involved a PES hollow ultrafiltration membrane as the pretreatment experiment of PAAS. It is clearly seen that free Zn (II) concentration measured by the permeate concentration decreases with the increase of the reaction time, reaches a minimum value and does not change again. It takes about 35 min for Zn (II) reach complexation equilibrium. This is similar to Zeng et al. [39]; it takes about 25 min and 50 min, respectively, for the dissociated polymer (PAA-) to complex completely with Hg (II) and Cd (II). Generally, it takes much less than 10 min for the fluid to leave the centrifugal pump to the membrane module in wastewater treatment; only a part of dissociated polymer can complex again with metal ions, causing remarkable reduction of rejection. Thus, it is necessary to study the shear stability of the polymer-metal complex for the industrial application of complexation-ultrafiltration.

CONCLUSIONS

The Removal of Zn (II) from aqueous solutions by a rotating disk shear enhanced complexation-ultrafiltration was studied, and the stability of PAA-Zn complex in the shear field was investigated for the first time. The optimal operation conditions of complexation-ultrafiltration were pH=7 and P/M=25, and the rejection of Zn (II) was 95.3% for 10 mg/L Zn (II) aqueous solution. The carboxylic group content of the PAA was calculated by titration, which was 7.672 mmol/L. The shear stabilities of PAA and PAA-Zn complex were studied. The polymer chain of PAA remains stable under 3,000 rpm whenever pH changes; however, the PAA-Zn complex will dissociate when the rotating speed exceeds a certain value, which depends on the pH. Low pH and high rotating speed can exacerbate the decomplexation of the PAA-Zn complex. The PAA-Zn complex will dissociate when the rotating speed is greater than 1,460, 1,390, 1,280 rpm at pH=7.0, 6.0, 5.0, and the critical shear rates (γ_c), the smallest shear rates at which the PAA-Zn complex begins to dissociate, were calculated by partition model: 1.58×10^5, 1.45×10^5 and 1.25×10^5 s^{-1} at pH 7.0, 6.0, 5.0, respectively. In addition, the relationship between the critical radius and the rotating speeds was obtained. The shear stability of polymer-metal complex is of great significance for the industrial application of complexation-ultrafiltration; it can give guidance for the selection of delivery pumps and rotating speed to avoid the polymer-metal complex from dissociating.

ACKNOWLEDGEMENT

This work was funded by the National Natural Science Foundation of China (Grant NO. 21476265).

NOMENCLATURE

Roman Letters

C_f : initial metal ions concentration [mg L^{-1}]
C_0 : metal ions concentration in permeate at rest [mg L^{-1}]
C_p : metal ions concentration in permeate [mg L^{-1}]
F : permeation coefficient [L m^{-2} kPa^{-1} h^{-1}, m s^{-1} Pa^{-1}]
J_p : permeate flux [L m^{-2} h^{-1}, m s^{-1}]
k : velocity following factor
N : rotating speed [rpm]
P_0 : center pressure [Pa]
P_p : peripheral pressure [Pa]
r_m : membrane outsider radius [m]
r_0 : membrane insider radius [m]
r_c : critical radius [m]
R_{Zn} : rejection of Zn (II) [%]
R_{PAAS} : rejection of PAAS [%]
R_t : total resistance [m^{-1}]
R_m : membrane resistance [m^{-1}]
R_f : membrane fouling [m^{-1}]
R_c : concentration polarization resistance [m^{-1}]
Re : Reynolds number
t : time [s]
V_p : permeate volume [L]

Greek Letters

μ : dynamic viscosity [Pa s]
ν : kinematic viscosity [m^2s^{-1}]
ρ : fluid density [kg m^{-3}]
γ_c : critical shear rate [s^{-1}]
γ_m : shear rate on membrane surface [s^{-1}]
γ_{mb}, γ_{mt} : shear rate on membrane surface in the laminar regime and turbulent regime [s^{-1}]
ω : angular velocity [rad s^{-1}]

REFERENCES

1. R. L. Ramos, L. A. B. Jacome, J. M. Barron, L. F. Rubio and R. M. G. Coronado, *J. Hazard. Mater.*, **90**, 27 (2002).
2. K. Anoop Krishnan, K. G. Sreejalekshmi, V. Vimexen and V. V. Dev, *Ecotoxicol. Environ. Saf.*, **124**, 418 (2016).
3. J. Zhang, Y. Li, J. Zhou, D. Chen and G. Qian, *J. Hazard. Mater.*,

205, 111 (2012).
4. S. Caprarescu, A. L. Radu, V. Purcar, R. Ianchis, A. Sarbu, M. Ghiurea, C. Nicolae, C. Modrogan, D. I. Vaireanu, A. Périchaud and D. I. Ebrasu, *Appl. Surf. Sci.*, **329**, 65 (2015).
5. H. G. Gorchev and G. Ozolins, WHO guidelines for drinking-water quality, *WHO Chron.* (2011).
6. J. Landaburu-Aguirre, E. Pongrácz, A. Sarpola and R. L. Keiski, *Sep. Purif. Technol.*, **88**, 130 (2012).
7. M. R. Awual, M. Ismael, T. Yaita, S. A. El-Safty, H. Shiwaku, Y. Okamoto and S. Suzuki, *Chem. Eng. J.*, **222**, 67 (2013).
8. M. E. Mahmoud, I. M. M. Kenawy, M. A. H. Hafez and R. R. Lashein, *Desalination*, **250**, 62 (2010).
9. F. Fu and Q. Wang, *J. Environ. Manage.*, **92**, 407 (2011).
10. M. Feizi and M. Jalali, *J. Taiwan Inst. Chem. Eng.*, **54**, 125 (2015).
11. K. R. Desai and Z. V. P. Murthy, *Chem. Eng. J.*, **185**, 187 (2012).
12. Y. Yurekli, *J. Hazard. Mater.*, **309**, 53 (2016).
13. Y. Zhang, S. Zhang and T. S. Chung, *Environ. Sci. Technol.*, **49**, 10235 (2015).
14. Y.-R. Qiu and L.-J. Mao, *Desalination*, **329**, 78 (2013).
15. D. J. Ennigrou, M. Ben Sik Ali and M. Dhahbi, *Desalination*, **343**, 82 (2014).
16. D. J. Ennigrou, M. Ben Sik Ali, M. Dhahbi and M. Ferid, *Desalin. Water Treat.*, **56**, 2682 (2015).
17. Y. Huang, D. Wu, X. Wang, W. Huang, D. Lawless and X. Feng, *Sep. Purif. Technol.*, **158**, 124 (2016).
18. H. Kim, K. Baek, B. K. Kim, H. J. Shin and J. W. Yang, *Korean J. Chem. Eng.*, **25**, 253 (2008).
19. R. Camarillo, J. Llanos, L. García-Fernández, Á. Pérez and P. Cañizares, *Sep. Purif. Technol.*, **70**, 320 (2010).
20. L. Zhao, H. Zhao, P. Nguyen, A. Li, L. Jiang, Q. Xia, Y. Rong, Y. Qiu and J. Zhou, *Desalination*, **322**, 113 (2013).
21. J. X. Zeng, H. Q. Ye, N. D. Huang, J. F. Liu and L. F. Zheng, *Chemosphere*, **76**, 706 (2009).
22. L. P. Buckley, S. Vijayan, G. J. McConeghy, S. R. Maves and J. F. Martin, *At. Energy Canada Limited, AECL*, **90**, 1544 (1990).
23. K. J. Hwang and S. J. Lin, *Chem. Eng. J.*, **244**, 429 (2014).
24. K. J. Hwang and S. E. Wu, *Chem. Eng. Res. Des.*, **94**, 44 (2015).
25. K. J. Hwang, S. Y. Wang, E. Iritani and N. Katagiri, *J. Taiwan Inst. Chem. Eng.*, **62**, 45 (2016).
26. W. Zhang, L. Ding, N. Grimi, M. Y. Jaffrin and B. Tang, *Sep. Purif. Technol.*, **175**, 365 (2017).
27. Z. Zhu, H. Mhemdi, W. Zhang, L. Ding, O. Bals, M. Y. Jaffrin, N. Grimi and E. Vorobiev, *Food Bioprocess Technol.*, **9**, 493 (2016).
28. S. Ladeg, Z. Zhu, N. Moulai-Mostefa, L. Ding and M. Y. Jaffrin, *Arab. J. Sci. Eng.*, **43**, 2237 (2018).
29. P. Meyer, A. Mayer and U. Kulozik, *Int. Dairy J.*, **51**, 75 (2015).
30. R. Bouzerar, M. Y. Jaffrin, L. H. Ding and P. Paullier, *AIChE J.*, **46**, 257 (2000).
31. R. Bouzerar, L. Ding and M. Y. Jaffrin, *J. Membr. Sci.*, **170**, 127 (2000).
32. M. Itoh, Y. Yamada, S. Imao and M. Gonda, *Exp. Therm. Fluid Sci.*, **5**, 359 (1992).
33. C. Torras, J. Pallarès, R. Garcia-Valls and M. Y. Jaffrin, *Desalination*, **200**, 453 (2006).
34. E. S. de Alvarenga, C. Pereira de Oliveira and C. Roberto Bellato, *Carbohydr. Polym.*, **80**, 1155 (2010).
35. P. Cañizares, A. Pérez, R. Camarillo and R. Mazarro, *J. Membr. Sci.*, **320**, 520 (2008).
36. G. Arthanareeswaran, P. Thanikaivelan, N. Jaya, D. Mohan and M. Raajenthiren, *J. Hazard. Mater.*, **139**, 44 (2007).
37. M. E. Romero-Gonzalez, C. J. Williams and P. H. E. Gardiner, *Environ. Sci. Technol.*, **35**, 3025 (2001).
38. M. Y. Jaffrin, *J. Membr. Sci.*, **324**, 7 (2008).
39. J. Zeng, H. Ye and Z. Hu, *J. Hazard. Mater.*, **161**, 1491 (2009).